Volume 13
Number 38
14 October 2022
Pages 5425-5516

Polymer Chemistry

rsc.li/polymers

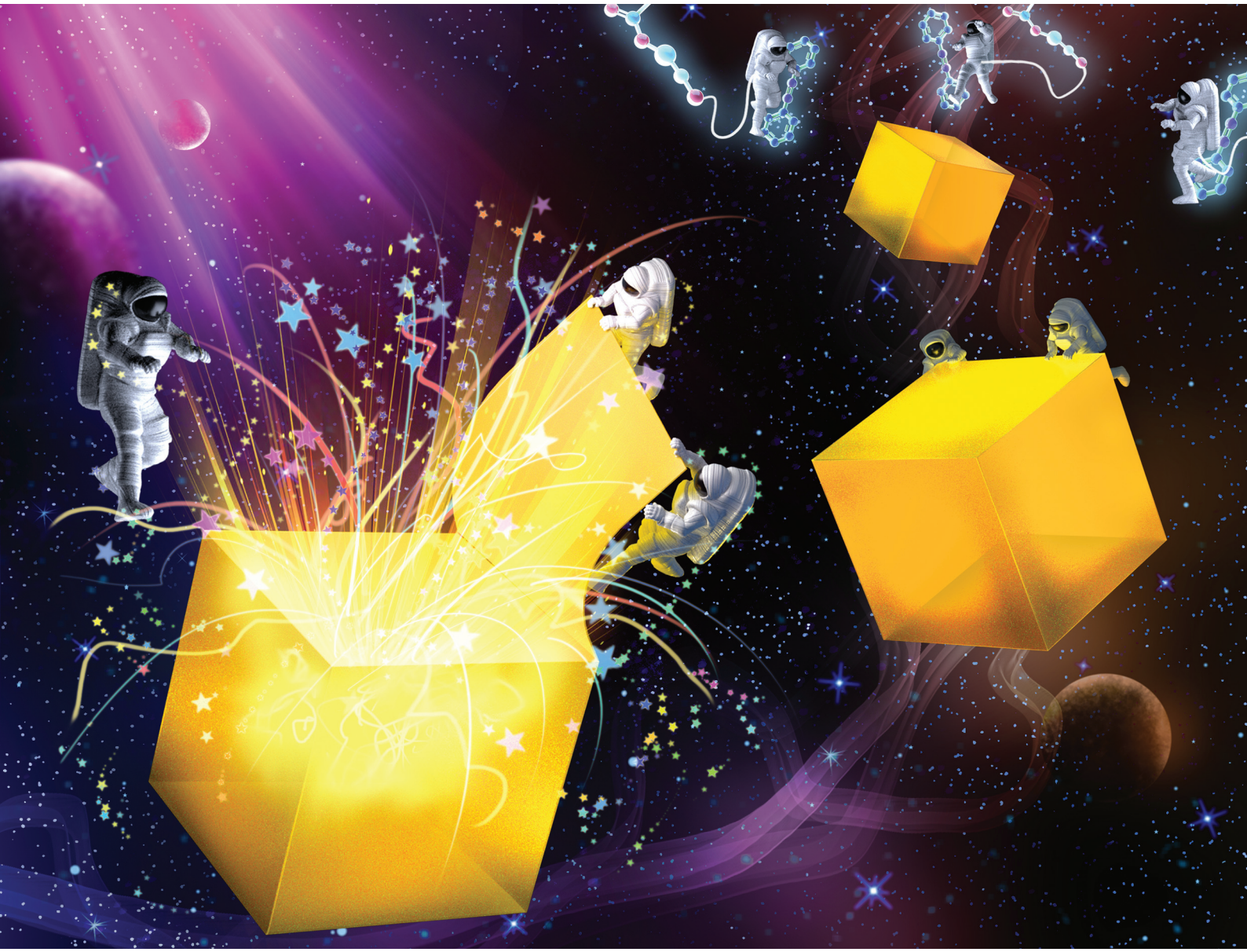

ISSN 1759-9962

ROYAL SOCIETY OF CHEMISTRY

COMMUNICATION
Jia Wei, Yanlei Yu *et al.*
Photoinduced deformation of amorphous polyimide enabled by an improved azobenzene isomerization efficiency

Polymer Chemistry

ROYAL SOCIETY OF CHEMISTRY

COMMUNICATION

View Article Online
View Journal | View Issue

Cite this: *Polym. Chem.*, 2022, **13**, 5447

Received 30th May 2022,
Accepted 23rd June 2022

DOI: 10.1039/d2py00691j

rsc.li/polymers

Photoinduced deformation of amorphous polyimide enabled by an improved azobenzene isomerization efficiency†

Xuejie Sun, Jia Wei * and Yanlei Yu *

Photodeformable azobenzene-containing polyimides (azo-PIs) have attracted attention due to their photo-response, good mechanical properties, and thermal stability. The deformation principle of azo-PIs mainly depends on the accumulation of conformational changes in one direction by polarized-light irradiation or pre-stretching. Herein, we synthesize a new deformable azo-PI and put forward a different strategy to achieve photodeformation by improving the azobenzene isomerization efficiency, which is attributed to the incorporation of azobenzene into the side chains of the polyimide (s-azo-PI). The s-azo-PI film exhibits reversible bending behaviour under alternate ultraviolet and visible light irradiation without using polarized light or pre-stretching. By means of this photodeformable behaviour, origami- or kirigami-inspired deformable 3D-structure objects, such as a cubic box and roller, are easily manufactured without any prior treatment, showing the potential to broaden the application of azopolymers in smart 3D actuators.

Photodeformable azobenzene-containing polymers (azopolymers) are intriguing due to their ability to undergo remote, localized, and wireless actuation under light irradiation.[1–4] In the past few decades, scientists have made tremendous efforts to develop azobenzene-containing liquid crystal polymers (azo-LCPs), in which photoinduced alignment changes of liquid crystal mesogens in the polymer networks caused a fast and large deformation.[5–12] By controlling the orientation of liquid crystal mesogens, azo-LCPs exhibit various deformation modes, including contraction,[9] bending,[13,14] twisting,[15] topographical deformation,[16,17] *etc*. To expand the use of photodeformable azopolymers under different conditions, researchers have developed some non-liquid-crystal azopolymers, such as azobenzene-containing polyimides (azo-PIs) with the advantages of photo-response, good thermal stability, and high mechanical strength.[18]

The photomechanical response of azo-PIs relies on the isomerization ability of azobenzene and the resulting conformational changes, bringing about local strain on the polymer networks.[19] However, due to the amorphous or semi-crystalline structures, the deformation of azo-PIs requires the accumulation of conformational changes in one direction, which is particularly important for producing enough contraction or expansion on the surface of materials to induce bending behaviour. To date, polarized light and pre-stretching have been used to orient azobenzene in a specific direction, leading to the accumulation of conformational changes.

The polarized-light-induced deformation of azo-PIs has been widely studied, in which the repeated *trans–cis–trans* isomerization causes the reorientation of azobenzene perpendicular to the polarization direction (the Weigert effect).[20–28] This reorientation process leads to the conformational changes of polymer networks in the polarization direction, thereby resulting in deformation. White *et al.* first synthesized a deformable polyimide with azobenzene as the crosslinker, and it exhibited a bending angle of ~20° after irradiation with polarized blue-green light for 30 min.[20] Subsequently, some efforts have been made to investigate the influence of the molecular structure on the photomechanical response of azo-PIs.[21–27] For example, freely rotating structures[24] or bulky substituents[25] increase the segmental mobility as well as free volume, which promotes the ability of azobenzene to undergo efficient reorientation and induce conformational changes, endowing azo-PIs with large deformation. However, as they lack the cooperative effect of azo-LCPs, the deformation of azo-PIs through reorientation is relatively slow, which is unfavourable for light-driven actuators.

The other way to achieve the deformation of azo-PIs is pre-stretching, which aligns random molecular chains along the external force direction.[28,29] Upon exposure to a light source, the aligned azobenzene simultaneously undergoes isomerization and conformational changes in the external force direc-

Department of Materials Science and State Key Laboratory of Molecular Engineering of Polymers, Fudan University, Shanghai 200433, China.
E-mail: weijia@fudan.edu.cn, ylyu@fudan.edu.cn

† Electronic supplementary information (ESI) available. See DOI: https://doi.org/10.1039/d2py00691j

tion. White *et al.* preceded in the fabrication of a pre-aligned azo-PI which demonstrated an increase in photoinduced stress and deformation speed.[28] Later on, our group reported a stretchable azo-PI with flexible linkers in the main chains. The stretched film showed fast bending behaviour based on the *trans–cis* isomerization of azobenzene under unpolarized ultraviolet (UV) light irradiation, and it reached a maximum bending angle of 112° in 8 s.[29] Pre-aligning azobenzene significantly improves the amplitude and speed of deformation. However, this method is only applicable to the stretchable azo-PIs. Besides, the necessary molecular alignment for fast deformation also poses additional challenges in constructing deformable 3D-structure objects, impeding their widespread use in diverse actuators. Thus, exploring a facile deformation method that breaks these limitations is meaningful, which will not only simplify the preparation process, but also make practical operation feasible.

Apart from the accumulation of conformational changes, the isomerization ability of azobenzene is another essential factor that influences the photodeformability of azo-PIs. A higher isomerization ability generates more conformational changes and strain on the polymer networks, providing an alternative design to realize the deformation of azo-PIs. Herein, we report a designed azo-PI with efficient azobenzene isomerization and explore its photodeformability triggered by unpolarized UV light irradiation as well as potential applications in actuators. Azobenzene is incorporated as part of the side chains into polyimide (s-azo-PI) in order to obtain a large free volume together with high azobenzene mobility, which is beneficial for *trans–cis* isomerization. The obtained s-azo-PI film, without pre-stretching, exhibits reversible bending behaviour upon UV and visible light irradiation, providing a facile route to deformable 2D/3D structures. Remarkably, we further demonstrate the potential use of s-azo-PI for manufacturing rotating or rolling actuators as well as smart origami-inspired objects.

In this work, a diamine monomer containing a side-chain azobenzene was designed. Meanwhile, a long flexible linker and ether linkage were introduced to increase the flexibility of molecular chains and lower the rotational barrier of benzene rings. The synthesis routes and chemical structures of the diamine monomer (s-DAC11AB) and the obtained polymer (s-DAC11AB-PI) are shown in Fig. 1a and b. The detailed experimental information and characterization are presented

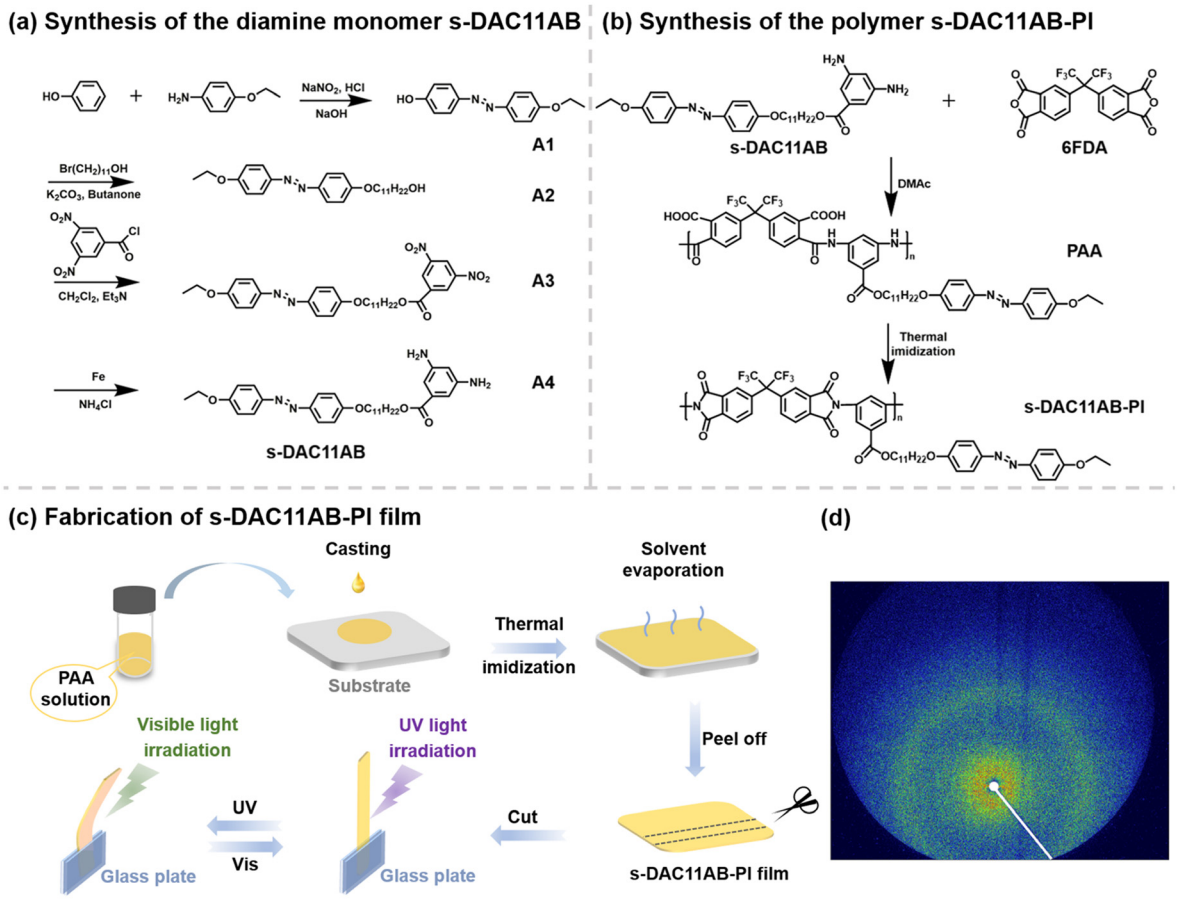

Fig. 1 (a) The synthesis route and chemical structure of s-DAC11AB. (b) The synthesis route and chemical structure of s-DAC11AB-PI. (c) Schematic diagram showing the fabrication and photoinduced deformation of the s-DAC11AB-PI film. (d) The 2D WAXD pattern of the s-DAC11AB-PI film showing the isotropic amorphous structure of the film.

in the ESI (Fig. S2 and S3†). The s-DAC11AB-PI film used to investigate photodeformability was prepared by a traditional two-step method (Fig. 1c), and possesses good thermal properties (T_g: ~147 °C by DSC, ~167 °C by DMA) and high mechanical strength with a storage modulus of 1.35 GPa (measured by DMA; Fig. S4†). 2D-WAXD was used to elucidate the isotropic characteristic of the film (Fig. 1d). The dispersive diffraction ring indicates the isotropic amorphous structure of the s-DAC11AB-PI film, which is consistent with that observed by POM (Fig. S5†).

Inspired by the origami method, we integrated a paper-folding step into the thermal imidization of poly(amic acid) (PAA) to shape 3D-structure objects so that the deformable azo-PIs actuator was no longer limited to 2D sheets. As shown in Fig. 2a, the PAA solution was cast onto the substrate and precured to form a PAA/PI film, which was manually folded into a cubic box and further imidized. Upon UV light illumination, the *trans–cis* isomerization of azobenzene on the surface of the film led to asymmetric contraction, causing the film to bend towards the light source. The asymmetric contraction is concerned with the changes in the chain stacking induced by the *trans–cis* isomerization of azobenzene on the surface of the film. The chain stacking of the s-DAC11AB-PI film before and after UV light irradiation was evaluated by wide-angle X-ray diffraction (WAXD). After UV light irradiation, 2θ becomes larger (from 17.8° to 18.4°) and the d-spacing becomes smaller (from 0.498 nm to 0.482 nm) (Fig. S6†). These changes indicate that the molecular chains stack more densely after UV light irradiation, which causes surface contraction on the side of the incident light. When irradiated with the visible light, the bent film went back to its initial state due to the *cis–trans* isomerization (Fig. 2b). As a result, the cubic box opened and closed with alternate UV and visible light irradiation (Movie S1†).

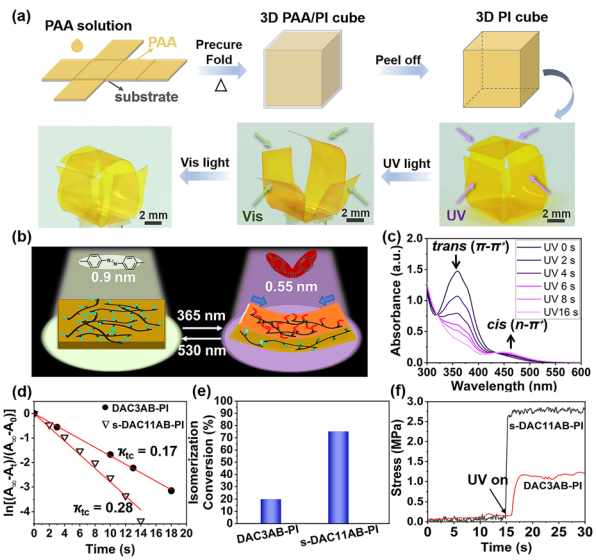

Fig. 2 (a) The fabrication scheme of a cubic box by integrating a paper-folding step into thermal imidization, and the light-controlled opening and closing behaviours of the obtained box under irradiation with UV and visible light. The cubic box size: 5 mm × 5 mm × 5 mm, thickness: 20 μm. UV light intensity: 70 mW cm^{-2}, visible light intensity: 80 mW cm^{-2}. (b) Schematic showing the deformation mechanism of the s-DAC11AB-PI film. (c) The UV-vis absorption spectrum of the s-DAC11AB-PI film under UV light (365 nm, 35 mW cm^{-2}) irradiation. The film thickness: ~3 μm. (d) The kinetic curves of the *trans–cis* isomerization of azobenzene in s-DAC11AB-PI and DAC3AB-PI films (red: fitting curve; black points: experimental data points). (e) The isomerization conversion of azobenzene in s-DAC11AB-PI and DAC3AB-PI films. (f) The photoinduced stresses of s-DAC11AB-PI and DAC3AB-PI films under UV light irradiation (365 nm, 70 mW cm^{-2}).

Different from previous works, the s-DAC11AB-PI film presented in this work exhibits reversible bending behaviour upon unpolarized UV/visible light irradiation without pre-stretching treatment, which is attributed to the efficient azobenzene isomerization and the large photoinduced stress, as illustrated in Fig. 2c–f. The isomerization ability depends on the environment of azobenzene and the connection of azobenzene with polymer chains. For comparison, a recently reported azo-PI with main-chain azobenzene (DAC3AB-PI) was synthesized (Fig. S1†), which showed poor deformability in the absence of pre-stretching (Fig. S7†).[29] Fig. 2c shows the photoisomerization of azobenzene in the s-DAC11AB-PI thin film under UV light irradiation. The changes in the absorption bands ascribed to the π → π* transition of the *trans* form and the n → π* transition of the *cis* form suggest the *trans–cis* isomerization of azobenzene. Notably, the absorption maxima of the π → π* transition change obviously after UV light irradiation, while those of the DAC3AB-PI thin film have a slight change (Fig. S8†), indicating that more azobenzene in the former undergoes isomerization. This is because azobenzene with a short flexible linker is constrained when bonded to rigid polymer main chains, making the *trans–cis* isomerization difficult.

The azobenzene isomerization makes the molecular length decrease from 9 Å to 5.5 Å. These conformational changes generate local strain and stress that are accumulated and transferred into macroscopic deformation. Therefore, to further elucidate the pivotal role of the *trans–cis* isomerization of azobenzene in the deformation, we calculated the first-order kinetic coefficient k_{tc}[30,31] and isomerization conversion.[32,33] Fig. 2c presents the kinetic curves of the *trans–cis* isomerization of azobenzene in the s-DAC11AB-PI and DAC3AB-PI thin films. The k_{tc} value of s-DAC11AB-PI is 0.28 s^{-1}, much larger than that of DAC3AB-PI (0.17 s^{-1}). This phenomenon stems from the fact that the side chains and long flexible linkers increase the free volume and flexibility of molecular chains, which is beneficial for azobenzene isomerization. The high mobility of side-chain azobenzene is conducive to the deformation of films, which was also reported in the previous work focusing on the polarized-light induced deformation of azo (polyamide imide)s.[34] Meanwhile, the isomerization conversion in the s-DAC11AB-PI film reaches up to 75% in the photostationary state, which is more than three times as large as that of the DAC3AB-PI film (~20%) (Fig. 2e). Thus, larger stress was generated in the s-DAC11AB-PI film (~2.6 MPa), two times that of the DAC3AB-PI film (Fig. 2f), causing the deformation

of the film even without pre-stretching. These results clearly prove that the side-chain azobenzene and long flexible linker significantly improve the photoisomerization ability, both of which are favourable to deformation.

The photodeformability and cycling performance of the s-DAC11AB-PI film were evaluated by testing the bending angle of the sample strip, as depicted in Fig. 3a and b. Upon exposure to UV light, the film bent toward the light source with a maximum bending angle of 70° in 65 s and then recovered to the initial vertical state in 17 s upon visible light irradiation (Fig. 3a and Fig. S9†). After 55 irradiation cycles, the maximum bending angle remains almost unchanged, indicating that the film possesses excellent anti-fatigue performance. Furthermore, the thermal relaxation behaviour of the UV-light-induced bending film shows a "photoplastic" feature.[35,36] After removing the UV light, the film reverted from 70° to 51° in 2 h and to 33° after 140 h in darkness (Fig. S10†).

Compared with the "photoplastic" response, the "photoelastic" relaxation[20] makes the photoinduced bending strip immediately return to its initial position once the irradiation stops, facilitating the construction and miniaturization of actuators. Constructing a bilayer structured film composed of non-responsive and photo-responsive films is a convenient approach to the actuators capable of autonomous movement under continuous illumination with UV light.[37–39] Consequently, we endowed the s-DAC11AB-PI film with a "photoelastic" characteristic by building a bilayer film composed of s-DAC11AB-PI and polyethylene (PE) layers through electrostatic binding. The obtained bilayer film presented repeatable photoelastic deformation, *i.e.*, the film bent quickly toward light upon UV light irradiation (1 s) and then automatically returned to its initial state (1 s) when the UV light was turned off (Fig. 3c and Movie S2†). These bending and recovery behaviours indicate that the generation and elimination of the force synchronized with UV light illumination. We also examined the influence of the PE film thickness on the deformation. The reduction in bending angle with the increased film thickness reflects the increasing resistance. Thanks to the large photoinduced stress, the bending angle was able to reach 25° and even the PE film thickness increased to 70 μm (Fig. 3d).

Benefiting from the automatic recovery of the composite film, different actuators made of the s-DAC11AB-PI/PE bilayer film were further explored. As shown in Fig. 4a and Movie S3,† a curled rotating actuator was designed, in which the contact area between the table and the head end of the actuator was larger than that of the tail end, causing greater friction at the head end. The curled actuator deformed to be straightened under the UV light irradiation. After removing the UV light, the straight actuator tended to return to its curled state. The recovery force overcame the smaller friction of the tail end and compelled the tail end to move forward while the head end stayed, eventually yielding a rotating motion. Moreover, the kirigami technique provides an alternative platform for building 3D-architecture actuators. We prepared a rolling robot with rectangular strips along the central axis of a cylinder on both sides by the kirigami technique (Fig. 4b). When the UV light was exerted from the left underside of the glass substrate, the lowest strips bent toward the substrate. The bending of strips yielded

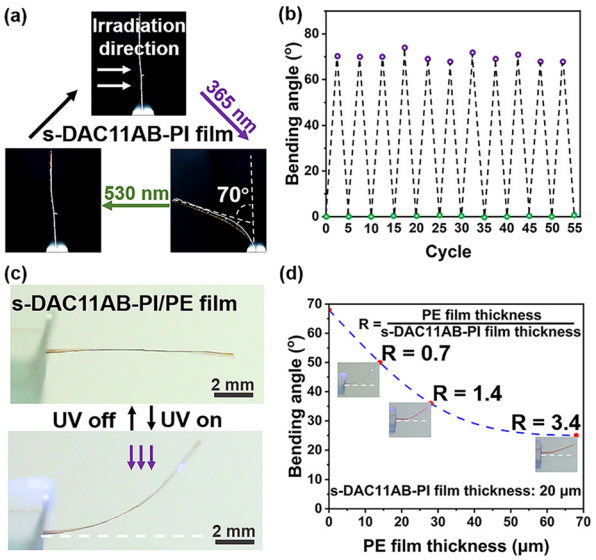

Fig. 3 (a) Photographs showing the bending and recovery behaviours of the s-DAC11AB-PI film (5 mm × 1 mm × 20 μm) upon UV and visible light irradiation. (b) The cycling performance for evaluating the bending and unbending deformation behaviours of the s-DAC11AB-PI film upon alternate irradiation with UV and visible light in 55 cycles. (c) The deformation behaviours of the s-DAC11AB-PI/PE bilayer film. The sample size is 10 mm × 2 mm and the s-DAC11AB-PI and PE film thickness is 20 μm and 14 μm, respectively. (d) The relationship between the bending angle and the PE film thickness under UV light irradiation. UV light: 365 nm, 70 mW cm^{-2}; visible light: 530 nm, 80 mW cm^{-2}.

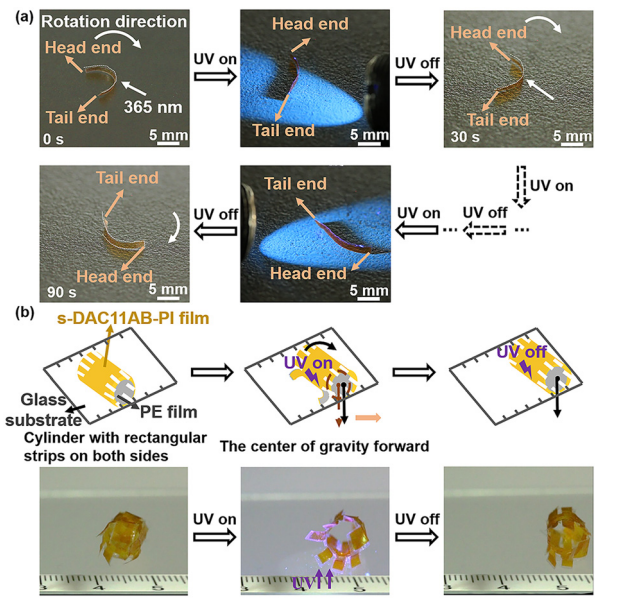

Fig. 4 (a) The rotating robot prepared using the s-DAC11AB-PI/PE film, which rotates on a rough surface under UV light irradiation. (b) Photographs of the rolling motion enabled by UV light irradiation from the underside of the glass substrate. UV light: 365 nm, 70 mW cm^{-2}.

enough stress to lift the robot up, which changed the gravity center and induced the robot to roll forward (Movie S4†).

In conclusion, we reported a straightforward way to prepare the photodeformable s-azo-PI based on the efficient photoisomerization of azobenzene and demonstrated its potential in constructing light-driven 3D actuators. Without the aid of prestretching, the amorphous s-azo-PI film was capable of bending under unpolarized UV light irradiation. This unexpected photodeformable behaviour is attributed to the large free volume in the polymer together with high azobenzene mobility. By means of this photodeformable behaviour, origami- or kirigami-inspired 3D-structure objects, such as a cubic box and roller, were easily manufactured and directly deformed under UV light irradiation without any prior treatment. This work developed a facile deformation strategy, which simplifies the processing and makes the deformable azo-PI actuators no longer limited to 2D structures like sheets, showing the potential to broaden the application of azopolymers in smart 3D actuators.

Experimental section

Materials

4,4′-(Hexafluoroisopropylidene)-diphthalic anhydride (6FDA) was purchased from Chinatech Chemical Co., Ltd. *N*,*N*′-Dimethylacetamide (DMAc), 3,5-dinitrobenzoyl chloride, 4-aminophenetole, phenol and iron were purchased from Adamas (Shanghai, China). 11-Bromo-1-undecanol was purchased from Aldrich. Other reagents were purchased commercially and used as received.

Synthesis of the monomer and polymer

Synthesis of the diamine monomer with side-chain azobenzene (s-DAC11AB). The s-DAC11AB monomer was synthesized in four steps, as shown in Fig. 1a. Briefly, A1 was synthesized *via* diazotization and intermediate A2 was obtained by the esterification of A1. The detailed synthetic routes to intermediates (A1, A2) were illustrated in our previous works.[40,41] Subsequently, 3,5-dinitrobenzoyl chloride was grafted to A2 through the esterification of acyl chloride with hydroxyl groups to obtain intermediate A3. Finally, the reduction of intermediate A3 was performed as described in the literature,[42] followed by the repeated extractions with dichloromethane. After chromatographic separation, a yellow solid of s-DAC11AB was obtained. Yield: 51%. ^{1}H NMR (500 MHz, CDCl3) δ: 7.88 (t, 4H), 7.0 (t, 4H), 6.80 (s, 2H), 6.18 (s, 1H), 4.29 (t, 2H), 4.05 (m, 4H), 3.70 (m, 4H), 1.89 ~ 1.31 (m, 18H), 1.27 (t, 3H).

Synthesis of the s-DAC11AB-PI film. The s-DAC11AB-PI film was prepared by the traditional two-step method. Briefly, a certain amount of s-DAC11AB (1 mmol) was added into a 50 mL three-necked flask with a magnetic stirrer. The DMAc solvent (18 mL) was injected into the flask through a syringe under a nitrogen atmosphere. After the s-DAC11AB monomer dissolved, 6FDA (1 mmol) was added to the above flask through a syringe under a nitrogen atmosphere. The mixture was then stirred at room temperature for 24 h to obtain viscous poly(amic acid) (PAA) solution. Next, PAA was cast on a glass substrate and thermally imidized at 80, 100, 150, 200, and 250 °C for 1 h, respectively. The obtained s-DAC11AB-PI film was peeled off from the substrate and washed with distilled water, followed by the drying process in an oven.

Fabrication of the rotating actuator with the s-DAC11AB-PI/PE bilayer film. The s-DAC11AB-PI film was cut into a strip and shaped into a curled shape. Then, the curled s-DAC11AB-PI film was stuck with PE film through electrostatic binding.

Fabrication of the rolling actuator with the s-DAC11AB-PI/PE bilayer film. A series of rectangle strips were cut on both sides of the s-DAC11AB-PI film and stuck with PE film. The s-DAC11AB-PI film with strips was then rolled up into a cylinder and fixed with glue.

Measurements

The ^{1}H NMR spectrum was obtained using a Bruker AVANCE III spectrometer (400 MHz, Karlsruhe, Germany) with deuterated chloroform ($CDCl_3$). Fourier transform infrared spectroscopy (FT-IR, VERTEX 70v, Germany) was used to analyze the molecular structures of s-DAC11AB and s-DAC11AB-PI, respectively. Differential scanning calorimetry (DSC) and dynamic mechanical analysis (DMA) were carried out on TA instruments Q2000 and Q800 (New Castle, DE, USA), respectively. The photoinduced stresses were measured using an Instron Universal Testing Machine (Model 5943) with a tensile rate of 1 mm min^{-1}. Ultraviolet-visible (UV-vis) absorption spectra were obtained using a Lambda 650 UV/VIS spectrometer (Waltham, MA, USA). The isotropic characteristic was measured using a polarized optical microscope (POM, Leica DM2500P) and two dimensional-wide angle X-ray diffractometer (2D-WAXD, Xeuss 2.0) with a 2D detector of Pilatus3R in transmission mode.

Conflicts of interest

There are no conflicts to declare.

Acknowledgements

This work was financially supported by the National Natural Science Foundation of China (no. 52073062).

References

1 T. Ikeda, J.-I. Mamiya and Y. L. Yu, *Angew. Chem., Int. Ed.*, 2007, **46**, 506–528.
2 J. Wei and Y. L. Yu, *Soft Matter*, 2012, **8**, 8050–8059.
3 X. L. Pang, J. A. Lv, C. Y. Zhu, L. Qin and Y. L. Yu, *Adv. Mater.*, 2019, **31**, 1904224.
4 M. E. McConney, A. Martinez, V. P. Tondiglia, K. M. Lee, D. Langley, I. I. Smalyukh and T. J. White, *Adv. Mater.*, 2013, **25**, 5880–5885.

5 M. Yamada, M. Kondo, R. Miyasato, Y. Naka, J.-I. Mamiya, M. Kinoshita, A. Shishido, Y. L. Yu, C. J. Barrett and T. Ikeda, *J. Mater. Chem.*, 2009, **19**, 60–62.
6 M. Yamada, M. Kondo, J.-I. Mamiya, Y. L. Yu, M. Kinoshita, C. J. Barrett and T. Ikeda, *Angew. Chem., Int. Ed.*, 2008, **47**, 4986–4988.
7 M. P. Cunha, E. A. J. Thoor, M. G. Debije, D. J. Broer and A. P. H. J. Schenning, *J. Mater. Chem. C*, 2019, **7**, 13502–13509.
8 Z. J. Wang, K. Li, Q. G. He and S. Q. Cai, *Adv. Mater.*, 2019, **31**, 1806849.
9 X. L. Pang, L. Qin, B. Xu, Q. Liu and Y. L. Yu, *Adv. Funct. Mater.*, 2020, **30**, 2002451.
10 H. Koerner, T. J. White, N. V. Tabiryan, T. J. Bunning and R. A. Vaia, *Mater. Today*, 2008, **11**, 34–42.
11 X. L. Pang, B. Xu, X. Qing, J. Wei and Y. L. Yu, *Macromol. Rapid Commun.*, 2018, **39**, 1700237.
12 F. J. Ge, R. Yang, X. Tong, F. Camerel and Y. Zhao, *Angew. Chem., Int. Ed.*, 2018, **57**, 11758–11763.
13 Y. L. Yu, M. Nakano and T. Ikeda, *Nature*, 2003, **425**, 145.
14 C. L. Oosten, C. W. Bastiaansen and D. J. Broer, *Nat. Mater.*, 2009, **8**, 677–682.
15 S. Iamsaard, S. J. Aßhoff, B. Matt, T. Kudernac, J. J. L. M. Cornelissen, S. P. Fletcher and N. Katsonis, *Nat. Chem.*, 2014, **6**, 229–235.
16 L. T. de Haan, C. Sanchez-Somolinos, C. M. W. Bastiaansen, A. Schenning and D. J. Broer, *Angew. Chem., Int. Ed.*, 2012, **51**, 12469–12472.
17 M. E. McConney, A. Martinez, V. P. Tondiglia, K. M. Lee, D. Langley, I. I. Smalyukh and T. J. White, *Adv. Mater.*, 2013, **25**, 5880–5885.
18 I. Gouzman, E. Grossman, R. Verker, N. Atar, A. Bolker and N. Eliaz, *Adv. Mater.*, 2019, **31**, 1807738.
19 K. M. Lee, D. H. Wang, H. Koerner, R. A. Vaia, L. S. Tan and T. J. White, *Angew. Chem., Int. Ed.*, 2012, **51**, 4117–4121.
20 D. H. Wang, K. M. Lee, Z. Yu, H. Koerner, R. A. Vaia, T. J. White and L. S. Tan, *Macromolecules*, 2011, **44**, 3840–3846.
21 B. K. M. Lee, H. Koerner, D. H. Wang, L. S. Tan, T. J. White and R. A. Vaia, *Macromolecules*, 2012, **45**, 7527–7534.
22 D. H. Wang, K. M. Lee, H. Koerner, Z. N. Yu, R. A. Vaia, T. J. White and L. S. Tan, *Macromol. Mater. Eng.*, 2012, **297**, 1167–1174.
23 D. H. Wang, J. J. Wie, K. M. Lee, T. J. White and L. S. Tan, *Macromolecules*, 2014, **47**, 659–667.
24 J. J. Wie, D. H. Wang, K. M. Lee, L. S. Tan and T. J. White, *Chem. Mater.*, 2014, **26**, 5223–5230.
25 M. L. Baczkowski, D. H. Wang, D. H. Lee, K. M. Lee, M. L. Smith, T. J. White and L. S. Tan, *ACS Macro Lett.*, 2017, **6**, 1432–1437.
26 D. H. Wang, K. M. Lee, D. H. Lee, M. Baczkowski, J. G. Lee, J. J. Wie and L. S. Tan, *ACS Appl. Mater. Interfaces*, 2021, **13**, 48127–48140.
27 D. H. Wang, K. M. Lee, D. H. Lee, M. Baczkowski, H. J. Park, M. E. McConney and L. S. Tan, *ACS Macro Lett.*, 2021, **10**, 278–283.
28 K. M. Lee, D. H. Wang, H. Koerner, R. A. Vaia, L. S. Tan and T. J. White, *Macromol. Chem. Phys.*, 2013, **214**, 1189–1194.
29 P. P. Zhang, Z. X. Lan, J. Wei and Y. L. Yu, *ACS Macro Lett.*, 2021, **10**, 469–475.
30 O. Tsutsumi, T. Shiono, T. Ikeda and G. Galli, *J. Phys. Chem. B*, 1997, **101**, 1332–1337.
31 J. Wang, Q. Jiang, X. T. Hao, H. C. Yan, H. Y. Peng, B. J. Xiong, Y. G. Liao and X. L. Xie, *RSC Adv.*, 2020, **10**, 3726–3733.
32 M. Higuchi, N. Minoura and T. Kinoshita, *Colloid Polym. Sci.*, 1995, **273**, 1022–1027.
33 Y. Kazushige, K. Katsushi and N. Hidehiko, *Bioorg. Med. Chem.*, 1999, **7**, 2977–2983.
34 A. K. Szmigiel, E. S. Balcerzak, D. Szmigiel and J. Konieczkowska, *J. Mater. Chem. C*, 2019, **7**, 4032–4037.
35 T. J. White, S. V. Serak, N. V. Tabiryan, R. A. Vaia and T. J. Bunning, *J. Mater. Chem.*, 2009, **19**, 1080–1085.
36 K. M. Lee, H. Koerner, R. A. Vaia, T. J. Bunning and T. J. White, *Macromolecules*, 2010, **43**, 8185–8190.
37 S. D. Ma, X. Li, S. Huang, J. Hu and H. F. Yu, *Angew. Chem., Int. Ed.*, 2019, **58**, 2655–2659.
38 X. Li, S. D. Ma, J. Hu, Y. Ni, Z. Q. Lin and H. F. Yu, *J. Mater. Chem. C*, 2019, **7**, 622–629.
39 J. C. Wang, S. Huang, Y. H. Zhang, J. G. Liu, M. M. Yu and H. F. Yu, *ACS Appl. Mater. Interfaces*, 2021, **13**, 6585–6596.
40 Y. L. Yu, T. Maeda, J. Mamiya and T. Ikeda, *Angew. Chem., Int. Ed.*, 2007, **46**, 881–883.
41 X. Zhang, C. Y. Zhu, B. Xu, L. Qin, J. Wei and Y. L. Yu, *ACS Appl. Mater. Interfaces*, 2019, **11**, 46212–46218.
42 A. B. Gambel, J. Garner, C. P. Gordon, S. M. J. Oconner and P. A. Keller, *Synth. Commun.*, 2007, **37**, 2777–2786.